Durable nanofluids-infused hierarchical surfaces with high corrosion and abrasion resistance

Shuqiang Wang[a], Shuxia Wang[b], Yanpeng Xue[a,*], Yanyan Xue[c], Quanyou Liu[d], Lili Cao[e], Mengyan Nie[f], Ying Jin[a*]

[a]National Center for Materials Service Safety, University of Science and Technology Beijing, Xueyuan Road 30, 100083, Beijing, China

[b]School of Management Science, Chengdu University of Technology, Chengdu, 610000, China

[c]School of Physics Science and Engineering, Institute for Advanced Study, Tongji University, Shanghai, 200092, China

[d]Testing Center of USTB Co., Ltd., Xueyuan Road 30, 100083, Beijing, China

[e]School of Mechanical and Energy Engineering, Zhejiang University of Science and Technology, Liuhe Road 318, Hangzhou, China

[f]Institute for Materials Discovery, University College London, Malet Place, London, WC1E 7JE, UK.

* Corresponding Author: yanpengxue@ustb.edu.cn; yjin@ustb.edu.cn.

Abstract:

Design of robust and durable ultra-lubricated surfaces having an efficient corrosion resistance ability is concerned in practical applications. Here a new optimized strategy to significantly improve the performance of ultra-lubricated surfaces by injecting slippery nanofluids into the hierarchical surfaces (SNHS) is proposed. In this work, cobalt-nickel hierarchical surfaces reinforced by micro SiO_2 particles were achieved on carbon steel substrate by electrochemical deposition and the functionalized nanofluids were injected into the hierarchical structure. Compared with nanostructured ultra-lubricated surfaces, SNHS exhibit better lubricity and corrosion resistance when subjected to water flow shear for more than 20 h. The tribo-electrochemical tests were

introduced to demonstrate that the SNHS has a lower coefficient of friction (0.39), more shallow wear marks (5 μm) and more complete surface morphology by directly comparing the wear resistance and self-healing ability. The hierarchical substrate has more advantages than the nanostructured substrate in the practical application of ultra-lubricated surface. Furthermore, the SNHS with robust mechanical durability can be a promising alternative technique for corrosion protection.

Keywords: Slippery liquid-infused porous surfaces; Co-Ni-based coating; Wear; Self-healing; Corrosion; Long-term stability;

1. Introduction

Recently, the anti-icing,[1–3] self-cleaning[4][5] and anti-corrosion[6–8] applications of super-hydrophobic surface inspired by the lotus-leaf have received extensively attention in industry and daily life.[9–12] However, these functional surfaces rely on the micro/nano structures to trap air, which causes unavoidable failure of its liquid-repelling performance under conditions of pressure and friction. To overcome the shortcomings of the super-hydrophobic surfaces, slippery liquid infused porous surfaces (SLIPS) are designed that lubricant liquid injected into the porous surface and exhibited antiwetting behavior. These surfaces display an ultra-lubricated and chemically continuous liquid lubricant interface that rapidly restores damaged areas through the fluidity of the liquid lubricant, providing inherent low hysteresis and self-healing properties.[13–15] Such functional surfaces show great application prospects in microbial corrosion inhibition[16–18] and energy harvesting. [19][20]

The formation of stable SLIPS requires chemically stable lubricating oil, as well as a structured surface to store lubricating oil and provide sufficient capillary force. However, the application of the SLIPS under actual working conditions faces environmental shear stresses to fluids, friction damage or the evaporation loss of liquid lubricant due to the continuous exposure to air, all of which affect the capillary phenomenon that holds the lubricant, leading to surface failure.[21] Based on this, a two-scale functional structure is proposed to prepare wear-resistant surfaces, where micro-

structures provide wear resistance and nano-structures provide water repellence. This strategy is applied in various materials and demonstrated universal applicability.[22][23] The micro-nano structure is effective to deal with the wear resistance, but it does not show any advantages for the protection of lubricating oil under water shear conditions. The effect of the micro-nanostructure length scale of the rough surface on the performance of SLIPS under fluid shear environment was investigated by Philseok Kim et al. The results demonstrated that micro-structured surfaces retained more lubricant but high-hysteresis than nano-structured surfaces after a high-spinning rate shear, which is attributed to the difficulty of micro-nano structures to provide sufficient capillary force on the upper layer of SLIPS.[24]

Recently, the functionalized nanofluids prepared by adding magnetic nanoparticles to lubricating oil has given SLIPS a broader application prospects in anti-icing and other fields.[25]–[29] Mixing perfluorinated ligands with other nanoparticles with which they can form strong interactions can significantly reduce the vapor pressure of the compounds. Perfluorinated ligands are used to create self-suspending nanoparticle fluids, which are used as lubricants in SLIPS to highly inhibit the evaporation rate. This strategy provides an approach for preparation of long-term stable SLIPS.[30]

In our previous work, wear-resistant micro-nano structured surfaces, including Co-Ni surface coatings,[31] Co-Ni/WC surface coatings and Co-Ni/CeO_2 surface coatings,[4][7] had been prepared by electrodeposition. Homogeneous solid solution Co-Ni-based coatings showed excellent wear resistance in the application of superhydrophobic surfaces. In order to obtain a SLIPS substrate with better comprehensive performance, it was further optimized on the basis of second phase particles on the surface of micro-nano structure, filling the gaps and increasing the capillary force.

Inorganic nanoparticles have good anti-friction and anti-wear properties, and their surface coated with long-chain organic molecules can form a stable mixture with lubricating oil.[32][33] Surface modified silane coupling agent can improve the dispersibility and stability of silica particles in a variety of organic solvents, and the

addition of lower concentrations can improve the wear resistance of the metal surface, which can be attributed to the formation of a deposited film of nano-silica on the interface, resulting in a rolling-ball effect.[34] This provides routes for the preparation of new functional nanofluids.

Hence, a new strategy is proposed that wear-resistant frameworks containing anti-friction nanofluids to comprehensively improve the performance of ultra-lubricated surfaces, including mechanical durability, corrosion resistance, water scouring resistance and low evaporation rate. Here, silica-filled wear-resistant Co-Ni-based coatings serves as a framework for storing nanofluids and self-suspended perfluorinated ligands-SiO_2 nanofluids as filling lubricant in hierarchical wear-resistant frameworks (SNHS). The wettability evolution of SNHS was recorded during water scouring process, and the corresponding electrochemical impedance spectroscopy (EIS) was also measured. The self-healing behavior of SNHS was investigated by measuring the tribo-electrochemical properties under corrosive solution as well as the topography and wear depth of the wear track after the wear process. As a contrast, nanostructured surfaces were injected with nanofluids (SNNS) to demonstrate the advantages of hierarchical micro-nano frameworks in terms of self-healing and resistance to water flow.

2. Experimental and Methods

2.1 Materials. Low-carbon steels (Q235) were purchased from bao shan iron & Steel Co., Ltd. and used as the substrate. The perfluoropolyether lubricant (PFPE, Krytox FSL 157) was purchased from Du Pont China Holding Co., Ltd. as a solvent for SiO_2 nanofluids. Other chemicals including cobalt chloride hexahydrate ($CoCl_2 \cdot 6H_2O$), boric acid (H_3BO_3), nickel chloride hexahydrate ($NiCl_2 \cdot 6H_2O$), perfluorooctyl trichlorosilane ($C_{48}H_4Cl_3F_{13}Si$, PFTEOS), hexadecyltrimethoxysilane ($C_{19}H_{42}O_3Si$, HDTMS) and two SiO_2 particles of different sizes (average diameter 5μm and 10 nm) were purchased from Shanghai yuanye Bio-Technology Co., Ltd.

2.2 Substrate surfaces preparation. Two types of SiO_2 particles were modified respectively before the preparation of two different types of substrate surfaces.

Chemical in situ synthesis was applied to obtain modified SiO_2 particles, where HDTMS and SiO_2 particles were added to the solvent and reacted at 50 °C for 5 h.

In order to obtain rough surfaces of different length scale, the electrochemical deposition was used to fabricate surfaces with different topography. The low-carbon steel was cut into substrate and used as the working electrode in a typical three-electrode system electrolytic cell, where the saturated calomel electrode (SCE), platinum sheet served as the reference electrode, counter electrode, respectively. Mixed deposition solution includes $NiCl_2 \cdot 6H_2O$ (0.04 mol/L), $CoCl_2 \cdot 6H_2O$ (0.2 mol/L), H_3BO_3 (0.2 mol/L) and 1g/L SiO_2 particles (average diameter 5 μm, modified by HDTMS). The Co-Ni/SiO_2 electrodeposits were obtained by controlling the constant current density of -10 mA/cm^2 or -50 mA/cm^2 for 1200 s to achieve nanostructured surface and micro-nano structured surface, respectively. The two as-deposited surfaces were immersed in 50 mL 10 wt.% PFTEOS ethanol solution for 20 min, then the samples were cleaned and heated at 50 °C for 2 h to obtain super-hydrophobicity.

2.3 Ultra-lubricated surface preparation. In this work, a simple method was applied to prepare self-suspending SiO_2 nanofluids as lubricants. Add modified SiO_2 particles (average diameter 10 nm, modified by HDTMS) to the PFPE and stir the mixture at high speed (1200 rpm) for 1 h. Then the mixed liquid was added to high-speed centrifuge for separation to remove the SiO_2 particles with a larger particle size in the bottom layer, and then a stable nanofluids can be obtained.

To form ultra-lubricated surfaces, the as-prepared nanofluids were painted on the two topographic surfaces and excess nanofluids were removed by tilting the surface at a small angle for several hours.

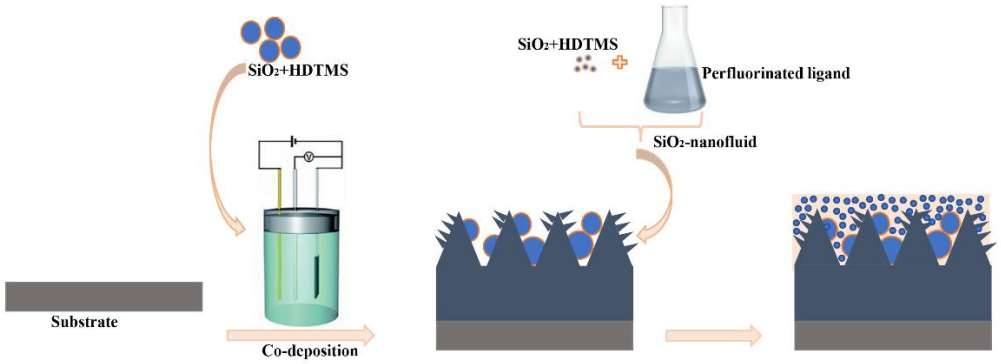

Figure 1. The fabrication process of nanofluids-infused hierarchical surfaces.

2.4 Microstructure, phase structure and chemical composition. FE-SEM (Hitachi S-5500) was performed to investigate the microstructure and cross-section of the sample surface. X-ray diffraction (XRD, Smart Lab 9 KW) was used to investigate the phase structure of the SiO_2 particles and composite surfaces. X-ray photoelectron spectrometer (XPS, Thermo Scientific Nexsa G2) was performed to reveal the surface chemical stages.

2.5 Wetting characterization. Automatic Contact Angle Test System (Model OCA200, DPIC) was applied to evaluate the surface wettability. The droplets volume was controlled around 5 μL and 12 μL respectively in the measurement process of WCA (water contact angle) and WSA (water sliding angle) and the average of three replicate experiments was used for data accuracy.

2.6 Tribo-electrochemical test. The tribological and self-healing properties of the SNNS and SNHS were evaluated in 3.5 wt.% NaCl solution using a tribo-electrochemical testing system (RETC MFT 5000). A constant load (5 N) was applied to a stainless-steel ball, which was rolled back and forth 5 mm on the specimen surface (20 mm × 20 mm) for 1200 s. Meanwhile, the open circuit potential (OCP), wear depth and friction coefficient were in-situ recorded. Confocal laser scanning microscope (CLSM, LEXT OLS4500) was performed to observe the morphology of the worn area after the tribo-electrochemical test.

2.7 Corrosion resistance test. The corrosion resistance evaluation was occurred in a typical three-electrode system electrolytic cell and measured values collected by

an Automatic Electrochemical Acquisition System (AEAS, Gamry-Reference 600). The surface to be tested acts as the working electrode in the electrolyte (1 M NaCl solution) more than 30 min to obtain the electrochemical system stable state before each test. Then the corrosion resistance measurements including potentiodynamic polarization curves (PPC) which recorded from -0.4 V to 0.5 V versus OCP (0.5 mV/s) as well as electrochemical impedance spectroscopy (EIS) which obtained from 10^5 to 10^{-2} Hz under the amplitude signal of 5 mV were conducted.

3. Results and Discussion

3.1 Characterization of SiO_2 nanofluids.

Evaporation rates of self-suspended perfluorinated nanoparticles were characterized by tracing the mass loss of SiO_2-nanofluids at 30 ℃ and 50 ℃ for up to 60 days. Two distinct phases of the evaporation processes can be observed in Fig. 2, where the relatively fast evaporation Phase I can be attributed to the volatilization of a small fraction of volatile impurities in the compound in the initial stage. In contrast, Phase II shows a constant and much lower evaporation rate than Phase I for all tested samples. As the temperature rises further, the evaporation loss increases significantly for both fluorinated ligand and nanofluids. But the evaporation loss of the nanofluids remains significantly lower than that of the ligand, which could be attributed to the formation of strong interactions between the fluorinated ligand and SiO_2 particles.[35]–[37] The combination of the dispersed solid phase (SiO_2 particles) and the perfluorinated ligand results in a negative mixing enthalpy (ΔH), which in turn results in a vapor pressure lower than an ideal mixture of the same composition.[30][38] The inset figure shows that the nanofluids still exist in a stable colloidal state after 60 days, which further proves the formation of a strong relationship between the two components.

The FTIR spectra (Fig. S1) of the perfluorinated ligand and the as-prepared SiO_2 nanofluids are compared to reveal the interaction between the nanoparticle and the ligand. In the 3000 ~ 4000 cm^{-1} range, the transmittance for both samples is >99, indicating the absence of water in the ligand as well as in the nanofluids. The peaks in the 1600 ~ 1800cm^{-1} range are instead attributed to the C=O stretching mode of

carboxylic acid. The C=O peak in the SiO_2 nanofluids shifts from 1770 cm^{-1} to 1683 cm^{-1} compared to the pure fluorinated ligand, which is attributed to the binding of carboxylate ions to metal sites on the nanoparticle surface, suggesting that the Krytox compound acts as a ligand on the particles.[30]

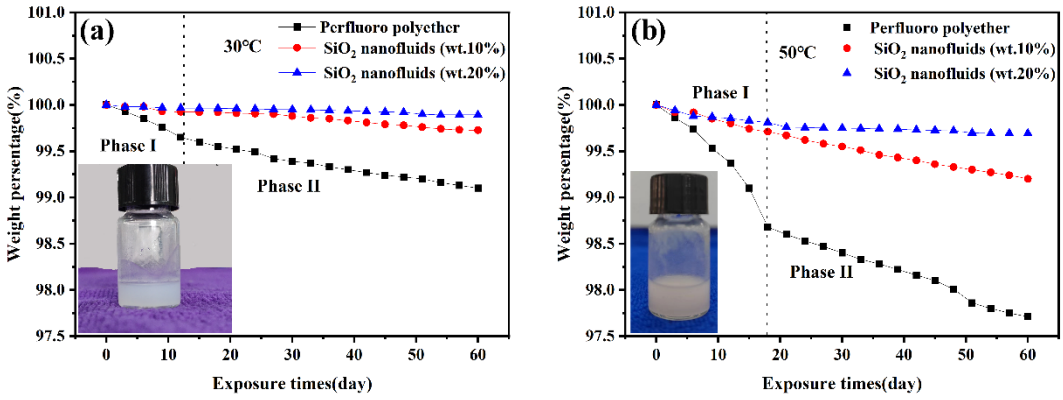

Figure 2. Evaporation loss of nanofluids with different SiO_2 mass fractions at: (a) 30 ℃ and (b) 50 ℃.

3.2 Porous surface morphologies of substrate coatings.

As shown in Fig. 3a-c, hierarchically structured Co-Ni/SiO_2 composite surfaces with the combination of nanometer and micrometer features, were prepared by electrodeposition technology. Micrometer features Co-Ni deposits as the basis of the micro-nano structure are uniformly distributed on the entire coating surface, and a large number of SiO_2 particles are filled in the gaps between the micro-structures (Fig. 3a). The micro-structured surfaces exhibit uniform nanoscale morphology crossed leaflets (Fig. 3c). As a control, by reducing the current density during the electrodeposition process, a uniform nano-scale cone-shaped surface doped with very small amount of SiO_2 particles was obtained (Fig. 3d-f). Compared with nano-structured surface, as-prepared surface of micro-nanostructures provides more space for storing lubrication oil, and the large amount of SiO_2 doping enlarges the contact area between the interface and lubrication oil and increases capillary action.

The cross-section images indicate that the thickness of the surface with hierarchical micro-nanostructures is around 50 μm, higher than that of the nano-structured surface (40 μm), which can be attributed to the higher current efficiency at the higher current

density. The higher overpotential leads to the formation of protrusion in the direction of increasing concentration.[6][35]

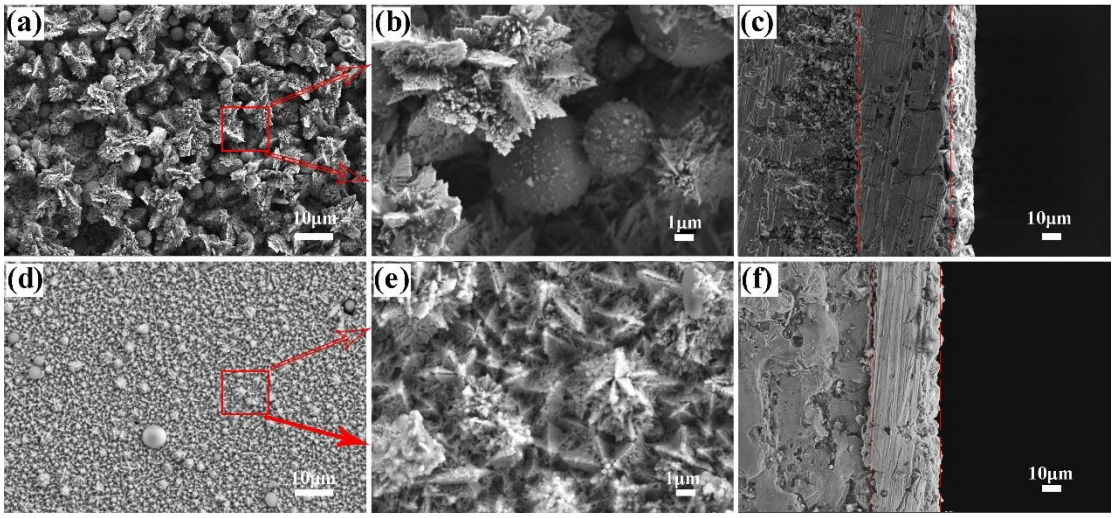

Figure 3. SEM images of (a,b) nanostructure surface deposited at -10 mA/cm^2 and its (c) cross section, (d,e) micro-nano hierarchical structured surface deposited at -50 mA/cm^2 and its (f) cross section.

3.3 Crystal structure and surface chemical compositions of substrate coatings.

The crystal structures and surface chemical composition of two structural surfaces were characterized by X-ray diffraction (XRD) and X-ray photoelectron spectroscopy (XPS) techniques, and shown in Fig. 4. Fig. 4a shows the XRD patterns of the micron-sized SiO_2 particles, nanostructured surface and micro-nano structured surface. The deposited Co-Ni alloy is homogeneous solid solution, which depicting a face-centered cubic (FCC) structure and a hexagonal close-packed (HCP) structure and no nickel peak is detected in the XRD pattern, which is consistent with our previous research results.[7][23] The uniform Co-Ni solid solution mixed with the second phase particles is an important method for forming a wear-resistant coatings.[4][7][31]

Fig. 4b shows the full XPS patterns of the modified micron-sized SiO_2 particles, modified nanostructured surface and micro-nano structured surface. Fig. 4bI shows strong signal of C1s, which could be attributed to the modified HDTMS. After the modification of PFTEOS, the nano-structured surface and micro-nano structured surface exhibit strong peaks of F1s (Fig. 4bII and III), which further confirmed of the

successful modification of the PFTEOS molecules. In addition, Fig. 4bIII also shows strong signals of C 1s, O 1s and Si 2s, which is due to a large amount of SiO_2 particles co-deposited on the surface of the micro-nano structures.

Fig. 4c depicts the high-resolution C 1s core level spectra of three kinds samples, and the strong signals at 284.4 eV could be attributed to the $(-Si(CH_3)_2O-)_n$ bond, which proves that the HDTMS molecules were successfully modified on SiO_2 particles (Fig. 4cI). The C1s core level peaks (Fig. 4cII and III) located at 282.8 eV, 288.7 eV, 291.1 eV and 293.6 eV could correspond to the -C-Si- group, $-C-CF_2-$ group, $-CF_2-$ group and $-CF_3$ group, revealing a successful modification of PFTEOS molecules on the surface.[39]

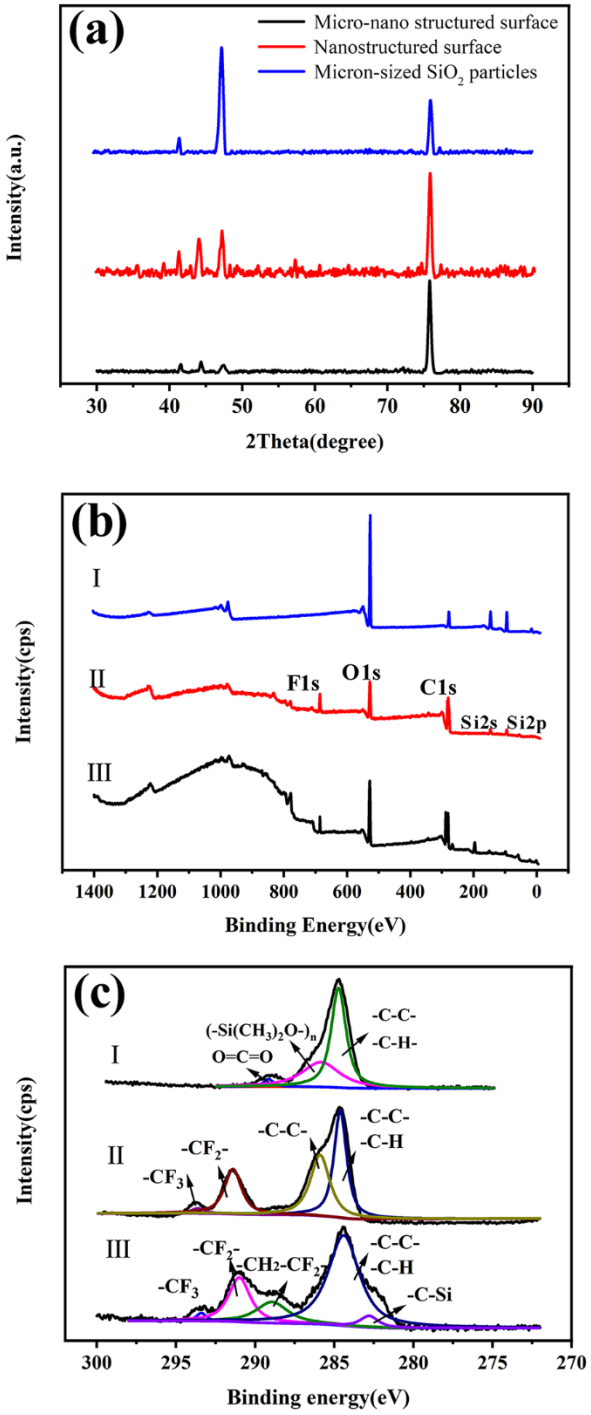

Figure 4. (a) XRD pattern and XPS spectra of micron-sized SiO_2 particles, nanostructured surface and micro-nano hierarchical histructured surface: (b) full XPS spectra and (c) high resolution C1s spectra.

3.4 Wettability of SNHS and SNNS.

The wettability of the SNNS and SNHS was investigated by static WCA and WSA measurements (Fig. 5a-b). The sliding processes of water droplet on two kinds of

surfaces were recorded as shown in Fig. 5c-d. The WCAs on the nano-structured surface are 112.3±1.5° and 163.7±0.5° before and after modification, which proves the hydrophobic transition of the surface (Fig. 5a). The WCAs on the micro-nano structured surface are 153.2±1° and 165.2±0.5° before and after modification, which shows that the super-hydrophobicity before modification is excellent, and the super-hydrophobicity is further improved after the modification (Fig. 5b). The WCAs on the SNHS and SNNS are 102.8±0.9° and 98.8±0.5°, indicating its similar property of hydrophobicity. Moreover, the water droplets gradually slid off from SNNS and SNHS after 4s, indicating their excellent self-lubricating performance and proving that the surface structure has no significant effect on the wettability of the ultra-lubricated surface (Fig. 5c-d).

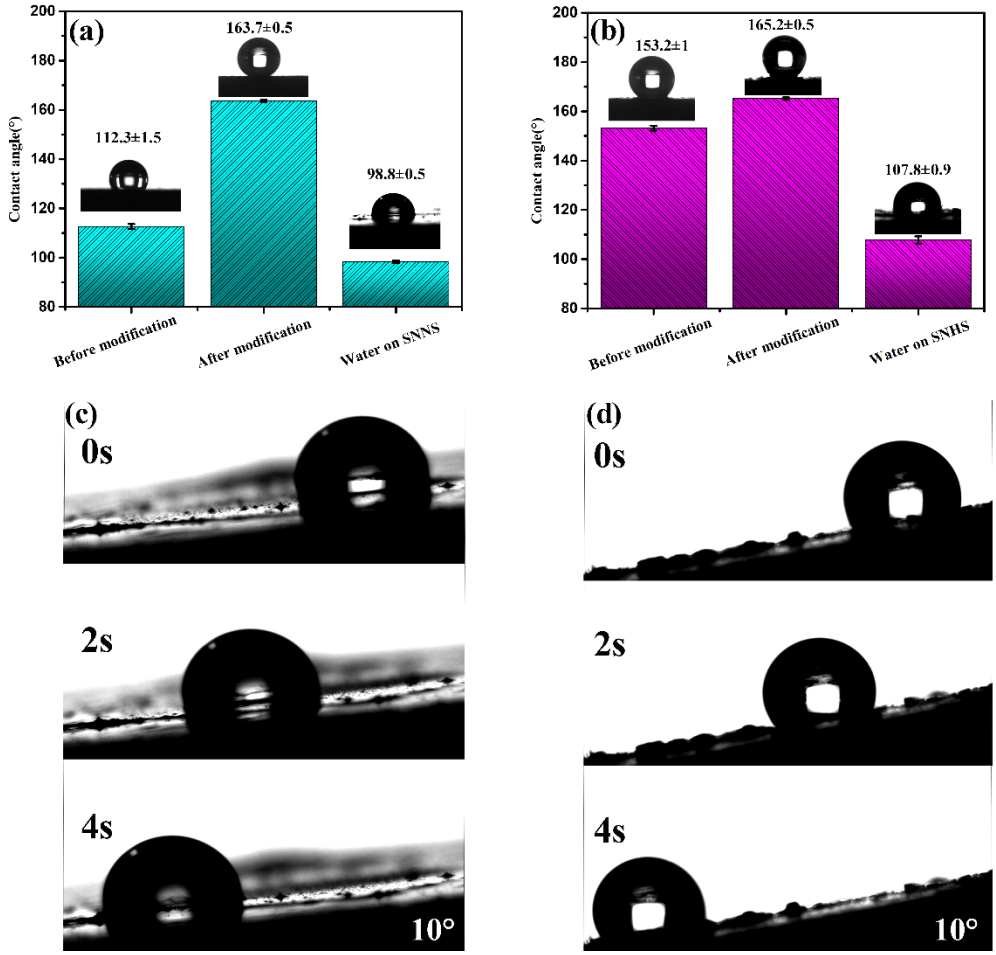

Figure 5. WCA of water (5 μL) droplets on the (a) nanostructured surface and SNNS, (b) micro-nano structured surface and SNHS; Sliding process of water droplet (10 μL) on (c) SNNS (c) and (d) SNHS.

3.5 Corrosion resistance of SNHS and SNNS.

The corrosion resistance of carbon steel substrate, nanostructured super-hydrophobic surface and SNNS, micro-nano structured super-hydrophobic surface and SNHS were investigated by potentiodynamic polarization curves (PPC) in 1 M NaCl aqueous solution, and shown in Fig. 6. Moreover, Tafel extrapolation was referenced to calculate the corrosion parameters including corrosion potential (E_{corr}), corrosion current density (i_{corr}) and corrosion rate and all values were given in Table 1. The PPC reveal that all the composite surfaces have much higher corrosion potential values and significantly lower corrosion current densities compared to bare carbon steel substrates. The positive shift of the E_{corr} value and the lower i_{corr} value are signatures of better corrosion resistance. Due to the hindering effect of trapped air, the i_{corr} values of the super-hydrophobic surfaces are reduced by an order of magnitude compared to the bare substrate, which could be attributed to the effectively reduced solution/solid contact area. Furthermore, the i_{corr} values of the nano-fluids-infused surfaces are almost one order of magnitude lower than those of the super-hydrophobic surfaces. Nanofluids infusion into the porous surface significantly suppressed the anodic and cathodic reactions of the corrosion process under the lubricating liquid, which further demonstrated that the infusion of nanofluids provides better corrosion inhibition than the air entrapment in the porous structures.[15] The i_{corr} value of the SNHS is 1.37×10^{-8} A/cm^2 and displays the best corrosion resistance comparing with other surfaces, which further demonstrates the better barrier effect of the infused nanofluids.

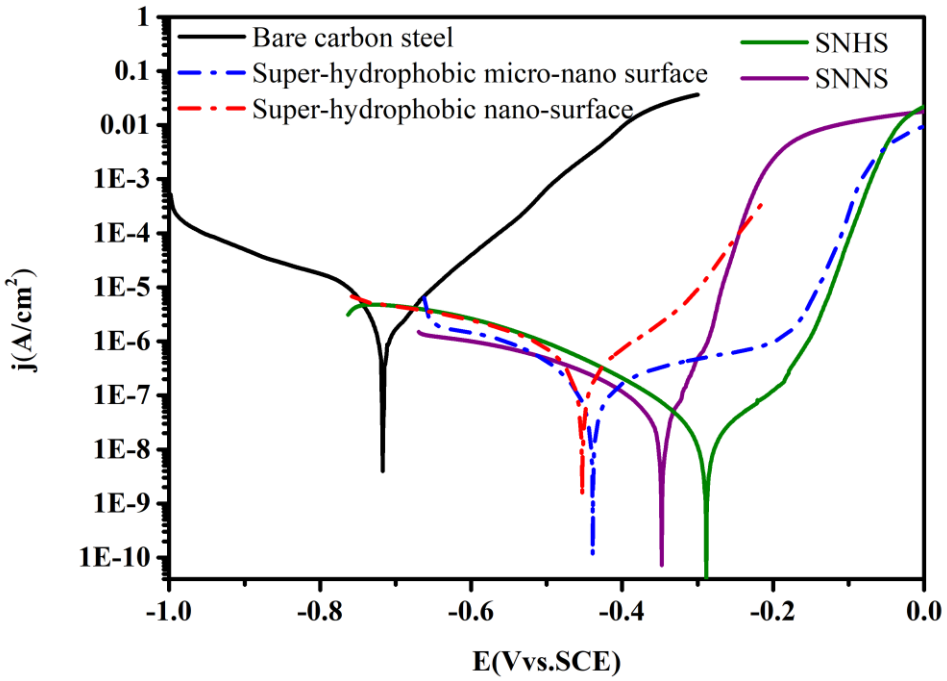

Figure 6. Potentiodynamic polarization curves of bare carbon steel, nanostructured super-hydrophobic surface and SNNS, micro-nano structured super-hydrophobic surface and SNHF in 3.5 wt.% NaCl aqueous solution at the scan rate of 0.5 mV/s.

Table 1. Results extracted from the potentiodynamic polarization measurements.

Samples	E_{corr} (mV)	i_{corr} (A/cm^2)	Corrosion rate(mm/a)
Bare carbon steel	-717.3	1.29×10^{-6}	0.0144
Super-hydrophobic nano-surface	-452.9	2.25×10^{-7}	0.0025
Super-hydrophobic micro-nano surface	-438.9	1.59×10^{-7}	0.0018
SNNS	-332.6	7.89×10^{-8}	0.0009
SNHS	-288.5	1.37×10^{-8}	0.0006

3.6 Self-healing properties and mechanical durability of SNHS and SNNS.

To assess the mechanical durability and self-healing behavior of the ultra-lubricated surfaces, the OCP values of the SNHS and SNNS were tracked in the corrosion medium before, during and after the wear process. It is pointed out in the literature that the open

circuit potential values are a mixed potential due to the complex state of the worn surface during the wear, which depends on the combined action of the active state of the material within the wear track and the passive state of the unworn region outside the wear track.[40] Before the wear process, the OCP values of two kinds of surfaces remained stable from 0 s to 600 s. Then, the OCP values suddenly dropped as the wear process begins, which was attributed to the temporary destruction of the super-lubricated surface. During the wear process, the OCP values gradually stabilized, indicating that the damage and self-healing process has reached a dynamic balance. When the wearing process ended, the OCP curves suddenly raised, but the OCP values were difficult to return to the initial level due to the permanent damage caused by the wear process. It should be pointed out that the SNHS exhibited better self-healing ability before and after the wear process, where the OCP values dropped by about 0.03V, which was less than the 0.08V of SNNS. The OCP value of SNHS recovered to around its original value abruptly after the wear process was terminated, while the recovery rate of SNNS was relatively slow. Fig. 7b shows more details of SNHS during the wear process. At 1200 s, the OCP value stabilized and periodically fluctuated in the subsequent wear process, due to the dynamic equilibrium of the damage-repair process.

Fig. 7c and 7d shows the recorded friction coefficient values (COF) of the wear process and the depth of wear track after testing. Among them, COF value reflect the maximum force at the friction interface.[41] As shown in Fig. 7c, the COF value of the tested samples shows periodic fluctuations during the cyclic sliding process, which may be attributed to the rough and hard substrate surface. The COF value of SNNS increased by about 0.05 over the entire test process and then stabilized around 0.44 in the regular reciprocating motion. This could be attributed to the difficulty of nanofluids filling the wore surface in time in the later stage of the test. The COF value of SNHS was stable around 0.39, and owing to the micro-nano surface stored more nanofluids layer and covering the rough surface in time. In contrast, the COF of the micro-nano surface covered by pure lubricant maintains a higher value of 0.6 and shows greater fluctuations than the nanofluids layer during the entire test, indicating that the nanofluids effectively

reduces the COF and fluctuations. The infused nanofluids formed a continuous liquid lubricant film that reduces the interfacial friction coefficient and protects the bare surface. In Fig. 7d, the wear depth of the SNHS and SNNS was close to 5 μm, and the wear depth of micro-nano surface covered by pure lubricant was close to 15 μm, which means that the presence of nanofluids significantly improves the wear resistance of the surface.

The worn surface morphologies of SNHS and SNNS were visually depicted by CLSM scans (Fig. 7e and 7f). The SNHS remained relatively intact and it was difficult to observe obvious signs of wear due to its low COF and the self-healing behavior. However, a wear depth about 5 μm could be observed on the SNNS due to the difficulty of storing large amounts of nanofluids on the nano-structured surface, which was difficult to cover the wear traces. In contrast, the wear-damaged SNHS could release more nanofluids in time and repair the defects to maintain the surface lubricated and alleviated further wear.

The wear resistance stability of the fabricated SNHS was further added and characterized by linear abrasion test (Fig. S3). A fixed pressure of 5 kPa was generated by the balancing weight to the 800 grit SiC sandpaper. The sandpaper was then pushed over the surface of the sample in remotion. The wear resistance stability of the sample was evaluated by measuring the sliding time at a sliding angle of 10° at different abrasion distances.

Within a linear abrasion distance of 16 m, the SNHS surface maintained a low sliding time and the contact angle increased by about 4.6°. When the linear abrasion distance exceeds 16 m, the sliding time increases sharply, and when the linear abrasion distance exceeds 28 m, the ultra-lubricated characteristic basically loses. Meanwhile, the SEM image shows the hierarchical structures and nanofluids were completely removed. From the obtained results, it can be observed that the critical value of the abrasion distance from which the loss of ultra-lubricated takes place is approximately 16 m.

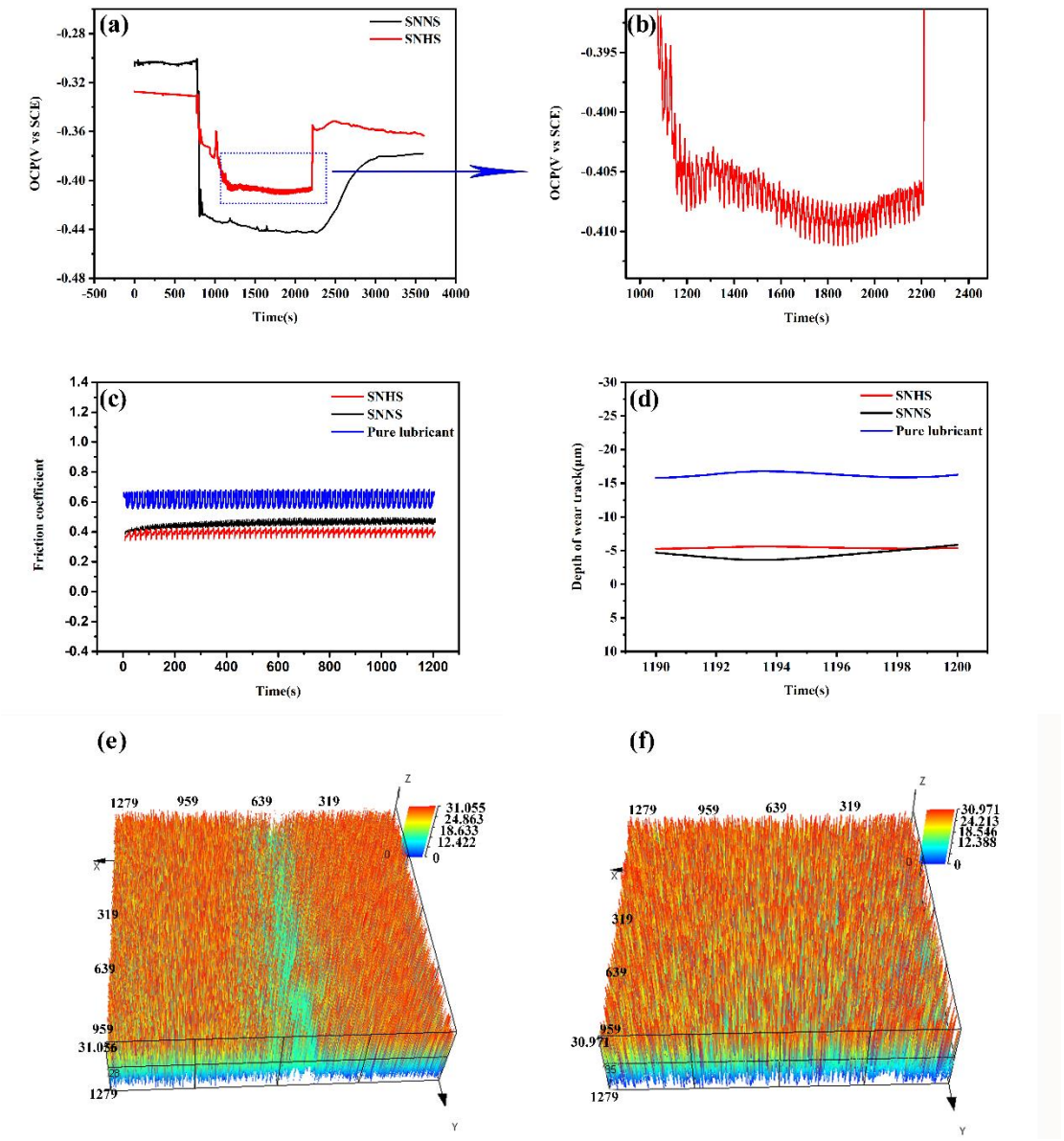

Figure 7. Tribological behaviors of SNNS and SNHS: (a,b) open circuit potential (OCP) before and after cyclic friction; (c) friction coefficient during the cyclic friction and (d) depth of wear track; CLSM image after wear of (e) SNNS and (f) SNHS.

3.7 Water scouring resistance of SNNS and SNHS.

The robustness of SNHS and SNNS were characterized by subjecting the coatings to high shear conditions and comparing the wettability of the surface. High-speed water flow was employed to simulate high shear conditions and the CAH value after scouring at a water flow velocity of 10.5 m/s for different time periods was recorded. As shown

in Fig. 8a, all samples show CAH of <7° for water droplets before the water flow scouring test. The CAH values of SNHS increased linearly in the early stage of water flow scouring, increasing from 4.8° to 13.4° in 6 h, which exhibited a rapid deterioration of slipperiness in the initial stage of scouring. In the subsequent 32 h water scouring test, the CAH value only increased slowly by about 4°. In contrast, the CAH value of SNNS remained basically unchanged with the increase of the water scouring time in the first 6 h of the test. Then, there was a sharp increase from 4.3° to 20.3° in CAH at 24 h indicating a rapid deterioration of slipperiness. In fact, the hierarchically structured ultra-lubricated surface (SNHS) provide advantage over the nanostructured ultra-lubricated (SNNS) in water repellent performance after shearing test for 20 h.

Fig. 8b shows the schematic diagrams of the evolution of the nanofluids profile and thickness with increasing scouring time. It is foreseeable that under long-term scouring conditions, ultra-lubricated surfaces with different surface structures would cause deterioration of wettability due to the lack of lubricants. SNNS shows obvious early advantages due to the more uniform surface structure, which provides effective capillary cation for locking the lubricant. However, under long-term scouring, the lubricant on the surface of SNNS is exhausted, resulting in deterioration of performance. The surface of SNHS stores more lubricant and the surface doped with SiO_2 particles effectively locks in the loss of lubricant, which shows more obvious advantages under long-term scouring conditions.

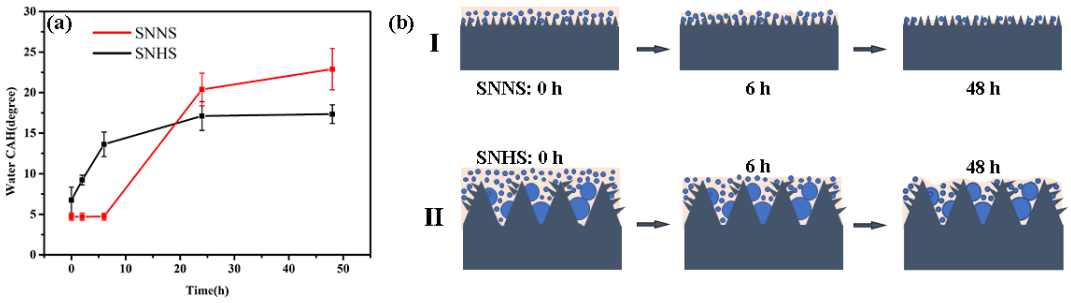

Figure 8. (a) Water contact angle hystereses (WCAH) on SNNS and SNHS after scouring for 50 hours at 2000 rpm; (b) Schematic diagrams of the evolution of the nanofluids profile and thickness with increasing scouring time on SNNS and SNHS.

The robustness of SNHS and SNNS are also characterized by comparing the corrosion resistance during the scouring process. Fig. 9 presents the EIS plots and their fitted results of two kinds of ultra-lubricated surfaces during the scouring conditions for 0 h, 2 h, 6 h, 24 h and 48 h. The semicircle Nyquist plots (Fig. 9a and 9d) of two surfaces show a typical behavior of solid metallic electrodes with the center below the real impedance axis. The size of the capacitive loop gradually decreased as the scouring time increased. Generally, the better anti-corrosion ability of a coating corresponded to the larger size of the capacitive loop. The Bode-module plots (Fig. 9b and 9e) show the impedance significantly drop in low frequencies region for the surfaces after scouring tests for 48 h, reflecting the loss of nanofluids in the barrier layer due to scouring process. The modular impedance (Z) at 0.01 Hz for the initial surface state of SNNS is as high as 1.98×10^3 kΩ·cm^2 but decreases gradually to 49 kΩ·cm^2 after scouring test. Interestingly, the values of $|Z|_{0.01Hz}$ are very close at 2 h, 4 h and 6 h, indicating little change in corrosion resistance. In contrast, the values of $|Z|_{0.01Hz}$ for SNHS are very close at 24 h and 48 h, which indicates the corrosion resistance is not significantly reduced in the long-term test for more than 24 hours. For two kinds of ultra-lubricated surfaces, the plots of phase angle (Fig. 9c and 9f) show three peaks in the region of intermediate and high frequencies are divided to correspond the corroding interface and the formation of ultra-lubricated surfaces. At higher frequencies, the phase angles continue to decrease during the scouring process for two kinds of ultra-lubricated surfaces.

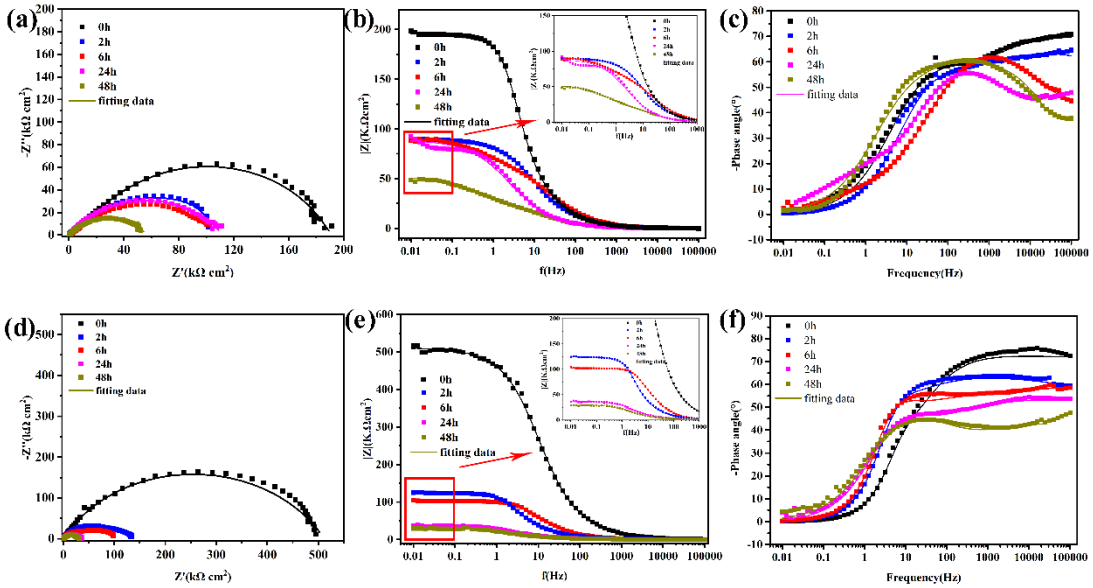

Figure 9. (a) EIS results of two types feature size ultra-lubricated surfaces during the water scouring process in 1 M NaCl solution: (a,d) Nyquist plots (b,e) Bode plots -|Z| and -phase angle versus frequency of SNNS; (c,f) Bode plots -|Z| and -phase angle versus frequency of SNHS.

In order to further analyze the corrosion principle of two kinds of ultra-lubricated surfaces during the scouring process, equivalent circuits in Fig. 10 are used to fit the EIS results. In this circuit, R_s, R_b and CPE_b represent the solution resistance, interface resistance and interface capacitance occurring at the interface of solution/ultra-lubricated surfaces, respectively. The R_c and CPE_c represent the porous resistance and porous capacitance occurring at the nanofluids/substrate interface. The R_{ct} and CPE_{dl}/C_{dl} represent charge transfer resistance and double layer capacitance occurring at ultra-lubricated surfaces/carbon steel substrate, respectively. The symbol CPE indicates the possibility of a non-ideal capacitance, which is considered to be a description of the relaxation time associated with heterogeneities at the surface of the electrode. From the literature,[23] the impedance of CPE is described as follows:

$$Z_{CPE} = 1/Y_0(j\omega)^n$$

where Z_{CPE} represents the impedance of a CPE, Y_0 represents the modulus, ω represents the angular frequency and n is the exponent of the CPE varying between 0 and 1.

Electrochemical parameters of SNNS during the scouring process are shown in Table 2, basing on the relevant equivalent circuits of Fig. 10b and 10c. The electrochemical parameters of SNHS, which based on the Fig. 10a, are summarized in Table 3. As shown in Table 3, the values of R_b and R_c drop by more than two orders of magnitude, while the values of R_c do not decrease significantly in the later stage of the scouring after 24h, indicating that although losing part of the nanofluids due to the shearing effect, SNHS still plays a good role in protecting the substrate. In contrast, R_c values of SNNS decrease from 294 kΩ·cm^2 to 23.0 kΩ·cm^2 and 0.633 kΩ·cm^2 with the scouring test time prolonged to 6 h and 24 h, which could be attributed to the large loss of nanofluids over the nano surface. In particular, when the scouring time reached to 48 h, R_{ct} values of SNHS are one order of magnitude higher than SNNS. This finding indicates that the SNHS shows a better corrosion protection in the long-term scouring conditions, where the nanofluids trapped in the micro-nano structures inhibiting the penetration of corrosive media into porous channels.

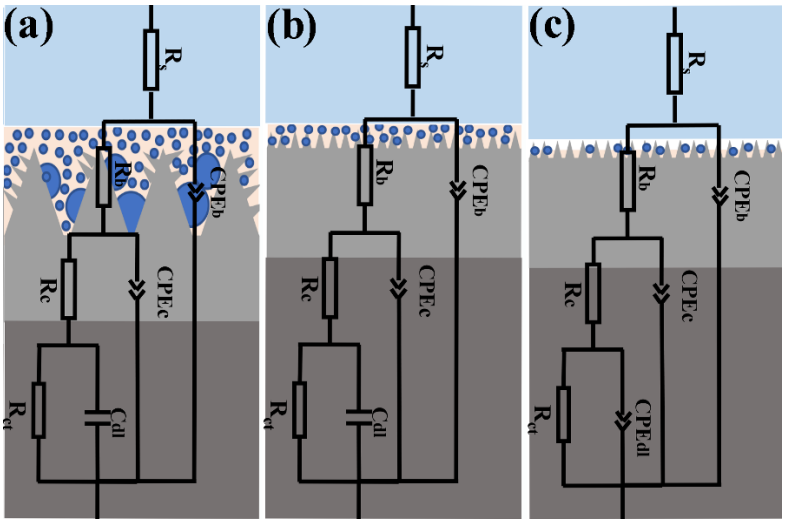

Figure 10. Equivalent circuits for fitting the EIS result of two types feature size ultra-lubricated surfaces during the scouring process (a) SNHS; (b,c) SNNS before and after scouring test.

Table 2. The impedance parameters of SNNS extracted by fitting the EIS results recorded in 1 M NaCl solution during the water scouring process.

Fitted Parameters	R_S	CPE_b	n_b	R_b	CPE_c	n_c	R_c	C/CPE_{dl}	n_{dl}	R_{ct}
SNNS-0h	6.42	1.65×10^{-8}	0.7759	2.94×10^{5}	7.48×10^{-9}	0.8241	2.72×10^{6}	5.20×10^{-8}	-	7.96×10^{5}
2h	7.41	5.23×10^{-8}	0.7677	8.36×10^{4}	2.01×10^{-8}	0.8165	2.11×10^{5}	4.14×10^{-8}	-	2.63×10^{5}
6h	9.32	2.80×10^{-7}	0.7271	2.30×10^{4}	1.11×10^{-7}	0.7856	5.15×10^{4}	8.56×10^{-6}	0.6837	4.17×10^{4}
24h	8.15	1.04×10^{-6}	0.6837	6.33×10^{2}	8.36×10^{-7}	0.7361	2.51×10^{4}	2.21×10^{-6}	0.6232	1.44×10^{4}
48h	14.54	2.17×10^{-5}	0.6706	1.10×10^{2}	1.44×10^{-4}	0.8742	6.31×10^{3}	4.32×10^{-5}	0.6102	2.11×10^{3}

Note: The units of R_s, R_{ct}, R_c and CPE are $\Omega\cdot cm^2$, $k\Omega\cdot cm^2$, $k\Omega\cdot cm^2$ and $\Omega^{-1}\cdot s^n\cdot cm^{-2}$, respectively.

Table 3. The impedance parameters of SNHS extracted by fitting the EIS results recorded in 1 M NaCl solution during the water scouring process.

Fitted Parameters	R_S	CPE_b	n_b	R_b	CPE_c	n_c	R_c	C_{dl}	R_{ct}
SNHS-0h	9.80	2.48×10^{-7}	0.8361	7.80×10^{5}	3.66×10^{-8}	0.8746	5.50×10^{5}	2.45×10^{-7}	4.08×10^{4}
2h	9.26	1.87×10^{-7}	0.8113	2.08×10^{4}	1.23×10^{-7}	0.8205	4.90×10^{5}	9.96×10^{-8}	1.49×10^{5}
6h	7.01	3.57×10^{-7}	0.7581	2.20×10^{4}	2.66×10^{-7}	0.8004	2.82×10^{5}	2.16×10^{-7}	9.79×10^{4}
24h	6.34	3.40×10^{-6}	0.6426	3.70×10^{3}	5.23×10^{-7}	0.8289	4.02×10^{4}	3.13×10^{-6}	2.47×10^{4}
48h	7.84	2.03×10^{-6}	0.6320	1.34×10^{3}	2.20×10^{-7}	0.8177	3.11×10^{4}	3.22×10^{-6}	2.07×10^{4}

Note: The units of R_s, R_{ct}, R_c and CPE are $\Omega\cdot cm^2$, $k\Omega\cdot cm^2$, $k\Omega\cdot cm^2$ and $\Omega^{-1}\cdot s^n\cdot cm^{-2}$, respectively.

4. Conclusions

A durable slippery nanofluids into the hierarchical surfaces (SNHS) was fabricated by injecting slippery functionalized nanofluids into the hierarchical wear-resistant Co-Ni-based frameworks. The SiO_2 nanofluids with anti-friction function shows low evaporation rate and high stability. SNHS maintains excellent lubricity and good corrosion resistance under the action of long-term water flow scouring. Compared with the nanostructured surface, the rationally modified micro-nano structured frameworks have more obvious advantages maintaining lubricity under long-term water scouring

conditions, which is helpful for the design of the durable ultra-lubricated surfaces. Tribological tests show that SNHS has a lower coefficient of friction (0.39), more shallow wear marks (5 μm) and more complete surface morphology. The linear abrasion test shows SNHS with lubricity for abrasion distance up to 16 m, indicating that the injection of nanofluids makes SNHS possessing excellent mechanical durability. Using micro-nano structured Co-Ni-based frameworks as nanofluids reservoirs, the SNHS exhibited significant corrosion resistance, self-healing ability and mechanical durability, which facilitates the application of ultra-lubricated surfaces in complex environments.

Acknowledgement

Dr. Xue thanks the support from Fundamental Research Funds for the Central Universities China (Project ID: FRF-TP-20-049A2). And the project was also supported by the Tribology Science Fund of State Key Laboratory of Tribology.

Conflict of Interest

The authors declare no conflict of interest.

References:

[1] F. Zhang, D. Xu, D. Zhang, L. Ma, J. Wang, Y. Huang, M. Chen, H. Qian, X. Li, *Chem. Eng. J.* **2021**, *423*.
[2] L. Ma, Z. Zhang, L. Gao, Y. Liu, H. Hu, *Renew. Energy* **2020**, *162*, 2344.
[3] P.W. Wilson, W. Lu, H. Xu, P. Kim, M.J. Kreder, J. Alvarenga, J. Aizenberg, *Phys. Chem. Chem. Phys.* **2013**, *15*, 581.
[4] Y. Xue, S. Wang, Y. Xue, L. Cao, M. Nie, Y. Jin, *Adv. Eng. Mater.* **2020**, *22*.
[5] J. Marlena, J.K.S. Tan, Z. Lin, D.X. Li, B. Zhao, H.L. Leo, S. Kim, C.H. Yap, *NPG Asia Mater.* **2021**, *13*.
[6] Y. Xue, S. Wang, G. Zhao, A. Taleb, Y. Jin, *Surf. Coatings Technol.* **2019**, *363*, 352.
[7] S. Wang, Y. Xue, C. Ban, Y. Xue, A. Taleb, Y. Jin, *Surf. Coatings Technol.* **2020**, *385*, 125390.
[8] Z. Shi, Y. Xiao, R. Qiu, S. Niu, P. Wang, *Surf. Coatings Technol.* **2017**, *330*, 102.
[9] X. Zhai, K. Li, F. Guan, C. Sun, J. Duan, B. Hou, *Surf. Coatings Technol.* **2018**, *344*, 259.
[10] X. He, P. Cao, F. Tian, X. Bai, C. Yuan, *Surf. Coatings Technol.* **2019**, *358*, 159.
[11] B. Zhang, J. Li, X. Zhao, X. Hu, L. Yang, N. Wang, Y. Li, B. Hou, *Chem. Eng. J.* **2016**, *306*, 441.
[12] Y. Zou, Y. Wang, S. Xu, T. Jin, D. Wei, J. Ouyang, D. Jia, Y. Zhou, *Chem. Eng. J.* **2019**, *362*,

638.
[13] K. Maji, A. Das, M. Dhar, U. Manna, *J. Mater. Chem. A* **2020**, *8*, 25040.
[14] C. Wang, Y. Yan, D. Du, X. Xiong, Y. Ma, *ACS Appl. Mater. Interfaces* **2020**, *12*, 29767.
[15] D. Wu, D. Zhang, Y. Ye, L. Ma, B. Minhas, B. Liu, H.A. Terryn, J.M.C. Mol, X. Li, *Chem. Eng. J.* **2019**, *368*, 138.
[16] P. Wang, Z. Lu, D. Zhang, *Corros. Sci.* **2015**, *93*, 159.
[17] P. Wang, D. Zhang, S. Sun, T. Li, Y. Sun, *ACS Appl. Mater. Interfaces* **2017**, *9*, 972.
[18] P. Wang, D. Zhang, Z. Lu, S. Sun, *ACS Appl. Mater. Interfaces* **2016**, *8*, 1120.
[19] W. Xu, X. Zhou, C. Hao, H. Zheng, Y. Liu, X. Yan, Z. Yang, M. Leung, X.C. Zeng, R.X. Xu, Z. Wang, *Natl. Sci. Rev.* **2019**, *6*, 540.
[20] Y. Song, W. Xu, Y. Liu, H. Zheng, M. Cui, Y. Zhou, B. Zhang, X. Yan, L. Wang, P. Li, X. Xu, Z. Yang, Z. Wang, *Innov.* **2022**, *3*, 100301.
[21] T. Wong, S.H. Kang, S.K.Y. Tang, E.J. Smythe, B.D. Hatton, A. Grinthal, J. Aizenberg, *Nature* **2011**, *477*, 443.
[22] D. Wang, Q. Sun, M.J. Hokkanen, C. Zhang, F.Y. Lin, Q. Liu, S.P. Zhu, T. Zhou, Q. Chang, B. He, Q. Zhou, L. Chen, Z. Wang, R.H.A. Ras, X. Deng, *Nature* **2020**, *582*, 55.
[23] C.N. Coatings, E. Deposition, S. Wang, Y. Xue, Y. Xue, C. Lv, Y. Jin, **2022**.
[24] P. Kim, M.J. Kreder, J. Alvarenga, J. Aizenberg, *Nano Lett.* **2013**, *13*, 1793.
[25] P. Irajizad, M. Hasnain, N. Farokhnia, S.M. Sajadi, H. Ghasemi, *Nat. Commun.* **2016**, *7*, 1.
[26] W. Wang, J.V.I. Timonen, A. Carlson, D.M. Drotlef, C.T. Zhang, S. Kolle, A. Grinthal, T.S. Wong, B. Hatton, S.H. Kang, S. Kennedy, J. Chi, R.T. Blough, M. Sitti, L. Mahadevan, J. Aizenberg, *Nature* **2018**, *559*, 77.
[27] M. Latikka, M. Backholm, J.V.I. Timonen, R.H.A. Ras, *Curr. Opin. Colloid Interface Sci.* **2018**, *36*, 118.
[28] N.N.M. Zawawi, W.H. Azmi, M.F. Ghazali, H.M. Ali, *Micromachines* **2022**, *13*, 1871.
[29] H. Babar, H. Wu, H.M. Ali, T.R. Shah, W. Zhang, *Int. J. Heat Mass Transf.* **2022**, *194*, 123085.
[30] X. Tian, S. Banerjee, I. Gonzalez-Alfonzo, L. Cademartiri, *Langmuir* **2020**, *36*, 5106.
[31] Y. Xue, S. Wang, P. Bi, G. Zhao, Y. Jin, *Coatings* **2019**, *9*, 1.
[32] D. Kim, L.A. Archer, *Langmuir* **2011**, *27*, 3083.
[33] D. Wu, L. Ma, F. Zhang, H. Qian, B. Minhas, Y. Yang, X. Han, D. Zhang, *Mater. Des.* **2020**, *185*, 108236.
[34] X. Li, Z. Cao, Z. Zhang, H. Dang, *Appl. Surf. Sci.* **2006**, *252*, 7856.
[35] P.H.C. Camargo, *J. Mater. Sci.* **2018**, 1.
[36] P. Agarwal, H. Qi, L.A. Archer, *Nano Lett.* **2010**, *10*, 111.
[37] R. Rodriguez, R. Herrera, L.A. Archer, E.P. Giannelis, *Adv. Mater.* **2008**, *20*, 4353.
[38] A.B. Bourlinos, A. Stassinopoulos, D. Anglos, R. Herrera, S.H. Anastasiadis, D. Petridis, E.P. Giannelis, *Small* **2006**, *2*, 513.
[39] F. Su, K. Yao, *ACS Appl. Mater. Interfaces* **2014**, *6*, 8762.
[40] A.C. Vieira, L.A. Rocha, N. Papageorgiou, S. Mischler, *Corros. Sci.* **2012**, *54*, 26.
[41] G. Lee, Y. Chan, S. Don, Y. Lee, *Curr. Appl. Phys.* **2011**, *11*, S182.